



CDF/ANAL/TOP/PUBLIC/10048
version 1.0
January 18, 2010

Measurement of $t\bar{t}$ Helicity Fractions and Spin Correlation Using Reconstructed Lepton+Jets Events

The CDF Collaboration¹

Abstract

Standard model top pair production produces a characteristic spin correlation which can be modified by new production mechanisms such as Z' bosons or Kaluza-Klein gluons. In the standard model, top quarks decay weakly before any hadronization processes take effect, enabling top spin information to be transmitted to the top quark decay products. We report on the observation and measurement of the $t\bar{t}$ helicity fractions and spin correlation in 4.3 fb^{-1} of $t\bar{t}$ reconstructed lepton+jet data. In the helicity basis, we find the opposite helicity fraction $f_o = 0.80 \pm 0.25(\text{stat}) \pm 0.08(\text{sys})$, and a spin correlation coefficient $\kappa = 0.60 \pm 0.50(\text{stat}) \pm 0.16(\text{sys})$.

¹<http://www-cdf.fnal.gov>

1 Introduction

This note presents a measurement of the $t\bar{t}$ spin state using a 4.3fb^{-1} lepton+jets sample collected by the CDF detector at the Fermilab Tevatron. In the standard model the top quark lifetime is shorter than the spin decoherence time, and the $t\bar{t}$ spin state at decay is mapped onto the V-A correlations in the final state. The $q\bar{q}$ annihilations that comprise $\sim 85\%$ of our sample should show the dominance of the $S = 1$ gluon annihilation channel. New physics could change this, and models of new physics appeal to the spin-correlation for signal identification and discrimination [1, 2].

The $t\bar{t}$ spin can be described by four helicity states $\bar{t}_L t_R, \bar{t}_R t_L, \bar{t}_L t_L, \bar{t}_R t_R$. In the $t\bar{t}$ rest frame the quarks move back-to-back and the same spin ($S = 1$) states are those with opposite helicity $\bar{t}_L t_R, \bar{t}_R t_L$. At threshold the opposite helicity fraction is 67%; at very high momentum helicity is conserved and this fraction rises to 100 [3, 4]. Integrating over all top momenta according to the pdf's and adding the small ($\sim 15\%$) $S = 0$ contribution from gg, we expect to find an opposite helicity fraction

$$f_o = \frac{\sigma(\bar{t}_R t_L) + \sigma(\bar{t}_L t_R)}{\sigma(\bar{t}_R t_R) + \sigma(\bar{t}_L t_L) + \sigma(\bar{t}_R t_L) + \sigma(\bar{t}_L t_R)} = \frac{N_o}{N_o + N_s} \approx 0.70. \quad (1)$$

where N_o and N_s are the numbers of opposite and same helicity events [3].

This analysis measures f_o by fitting the helicity angle bilinears $\cos(\theta_l) \cos(\theta_d)$ and $\cos(\theta_b) \cos(\theta_d)$ to the sum of template distributions for the four $t\bar{t}$ helicity eigenstates. Since CP conservation implies $\sigma(\bar{t}_R t_R) = \sigma(\bar{t}_L t_L)$, the same helicity (SH) template shape is symmetric sum of $\sigma(\bar{t}_R t_R) + \sigma(\bar{t}_L t_L)$. Since P conservation implies $\sigma(\bar{t}_R t_L) = \sigma(\bar{t}_L t_R)$, the opposite helicity (OH) template shape is the symmetric sum of $\sigma(\bar{t}_R t_R) + \sigma(\bar{t}_L t_L)$. The helicity angle bilinears are fit to the sum of the OH and SH templates and we measure the opposite helicity fraction f_o as above.

The $t\bar{t}$ spin state is often discussed in terms of the spin-correlation parameter

$$\kappa = \frac{[\sigma(\bar{t}_R t_L) + \sigma(\bar{t}_L t_R)] - [\sigma(\bar{t}_R t_R) + \sigma(\bar{t}_L t_L)]}{\sigma(\bar{t}_R t_R) + \sigma(\bar{t}_L t_L) + \sigma(\bar{t}_R t_L) + \sigma(\bar{t}_L t_R)} = \frac{N_o - N_s}{N_o + N_s}. \quad (2)$$

which is simply related to the opposite helicity fraction $f_o = \frac{1}{2}(1 + \kappa)$. For uncorrelated spins, $\kappa = 0$, and $f_o = 0.5$. A recent and elegant CDF measurement [5] uses kinematic reconstruction in the dilepton sample to find the lepton and b-quark helicity angles in the off-diagonal basis [4] and then fits the 2D distributions of these angles to the expected functional form. In 2.8fb^{-1} of data this yields $\kappa = 0.32^{+0.55}_{-0.78}$.

2 Data Sample and Event Selection

We analyze a 4.3fb^{-1} dataset in the lepton+jets channel, consisting of a total of 1001 events. The event selection requires one central lepton with large transverse momentum, missing transverse energy of at least 20 GeV, and 4 or more tight jets, at least one of which must be tagged as a b jet. The background is calculated using a

combination of Monte Carlo samples and data samples, with a predicted total of 215 ± 48 background events. For details of the event selection and background calculation, see [6].

Our analysis revolves around the correlation of the helicity angles of the lepton and the down and bottom quarks coming from the hadronically decaying top. The helicity angle, defined as the angle between the decay product momentum (in the top rest frame) and the top quark momentum (in the $t\bar{t}$ rest frame) carries information about the spin of the parent top quark. In order to validate our event selection and background model, we look at the cosines of these three helicity angles in Figures 1 through 3. In these figures, our selected data sample is compared to the sum of our background model and a $t\bar{t}$ signal sample created using PYTHIA, which does not contain a spin correlation effect.

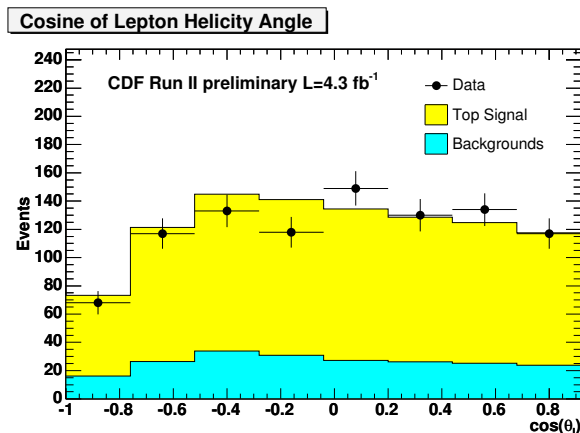


Figure 1: Distribution of $\cos(\theta_l)$ variable in data compared to the sum of our background model (light blue) and a PYTHIA signal model (yellow).

We validate our background model by comparing the predicted shape to the background rich sample with no b-tags (the “anti-tag” sample). Figure 4 shows the product $\cos(\theta_l)\cos(\theta_d)$ for the anti-tag sample, compared to our background model summed with the small expected contribution from $t\bar{t}$ events, modeled by PYTHIA. The model is seen to be a good reproduction of the data.

3 Template Creation and Measurement Method

3.1 Same Helicity and Opposite Helicity Templates

We use a binned likelihood template fit which requires same helicity and opposite helicity templates in order to perform a fit to the data. These templates were created using a modified version of the HERWIG Monte Carlo generator.

In top quark decays, the angular distributions of the top decay products determined by the helicity of the parent top quark via Equation 3

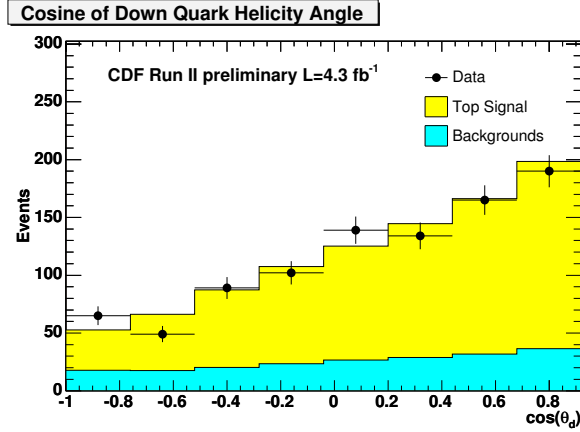


Figure 2: Distribution of $\cos(\theta_d)$ variable in data compared to the sum of our background model (light blue) and a PYTHIA signal model (yellow).

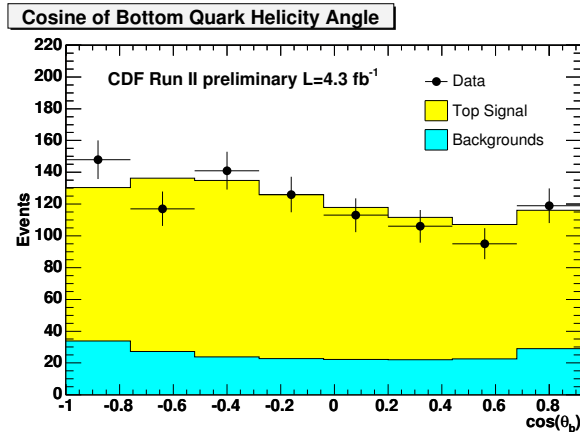


Figure 3: Distribution of $\cos(\theta_b)$ variable in data compared to the sum of our background model (light blue) and a PYTHIA signal model (yellow).

$$f(\cos(\theta_i)) = \frac{1}{2}(1 \pm A_i \cos(\theta_i)) \quad (3)$$

where the positive sign is for right-handed top quarks and the negative sign refers to left-handed top quarks (the signs are reversed for antitop decays). The correlation coefficient A_i varies for each decay product, being equal to +1.0 for the charged lepton or down quark, -0.41 for the bottom quark, and -0.31 for the neutrino or up quark [4].

We created our templates by modifying the HERWIG source code to implement this angular distribution for the charged lepton or down type quark, and then allowing the internal HERWIG machinery to propagate the appropriate angular distributions to the other decay products. Using this modified HERWIG, we then created four different simulated Monte Carlo samples, corresponding to the four possible top pair helicity states, $\bar{t}_L t_R, \bar{t}_R t_L, \bar{t}_L t_L, \bar{t}_R t_R$. Figures 5 through 7 show the truth-level angular distributions for

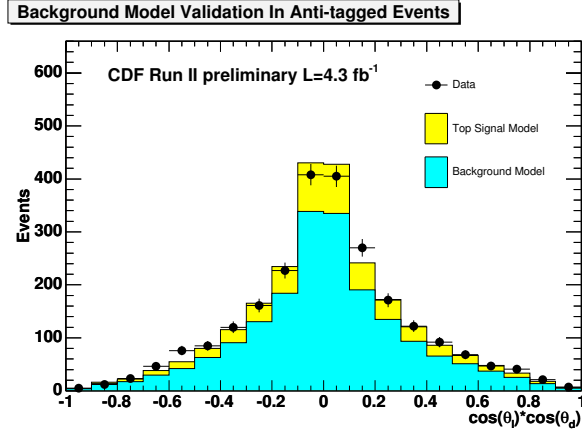


Figure 4: Distribution of $\cos(\theta_l) \cos(\theta_d)$ variable in anti-tagged data sample compared to the sum of our background model (light blue) and a PYTHIA signal model (yellow).

the top quark decay products for these four helicity samples, while Figures 8 through 10 show the same for the antitop quark decay products. In all cases, the expected slopes are observed.

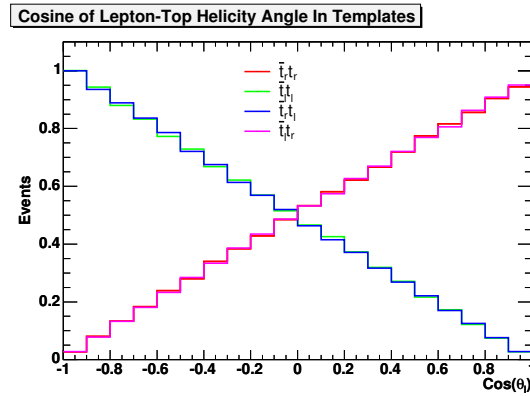


Figure 5: Distribution of $\cos(\theta_l)$ variable in top quark decays at truth level for our four samples representing the four different top pair helicity states. The samples show the expected slopes of +1 for right-handed tops and -1 for left-handed tops.

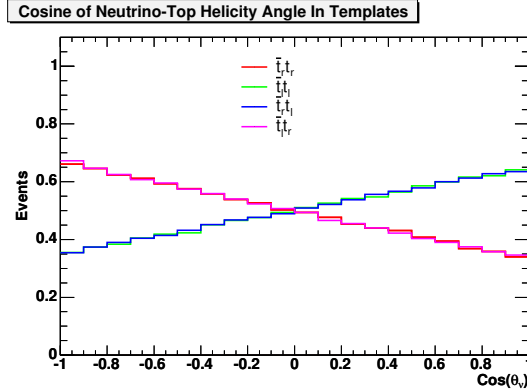


Figure 6: Distribution of $\cos(\theta_\nu)$ variable in top quark decays at truth level for our four samples representing the four different top pair helicity states. The samples show the expected slopes of -0.31 for right-handed tops and $+0.31$ for left-handed tops.

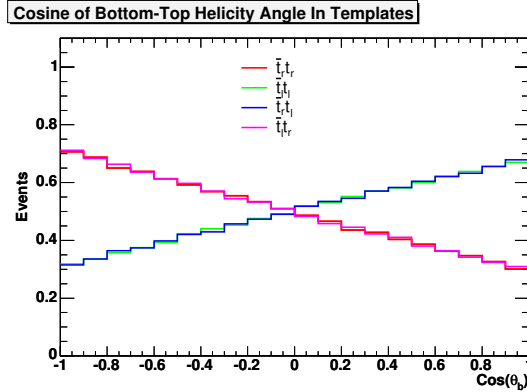


Figure 7: Distribution of $\cos(\theta_b)$ variable in top quark decays at truth level for our four samples representing the four different top pair helicity states. The samples show the expected slopes of -0.41 for right-handed tops and $+0.41$ for left-handed tops.

With the simulated samples prepared for the four different top pair helicity states, templates were created by combining the $\bar{t}_L t_R$ and $\bar{t}_R t_L$ samples in equal ratios according to parity conservation to form an opposite helicity sample and combining the $\bar{t}_L t_L$ and $\bar{t}_R t_R$ samples in equal ratios according to CP conservation to form a same helicity sample. To show the effect of the top quark helicity states on the distributions of interest in this analysis, Figures 11 and 12 show the variable $\cos(\theta_l) \cos(\theta_d)$, comparing the distribution at truth level in HERWIG without spin correlations to the same and opposite helicity templates respectively.

Figures 11 and 12 assume that the down quark can be identified 100% efficiently, but one of the difficulties of this analysis is that this is not the case. In order to choose the down quark, we use the prescription described in [4]: the jet closest to the b jet in the W rest frame will be the d jet approximately 60% of the time. Figures 13 and 14

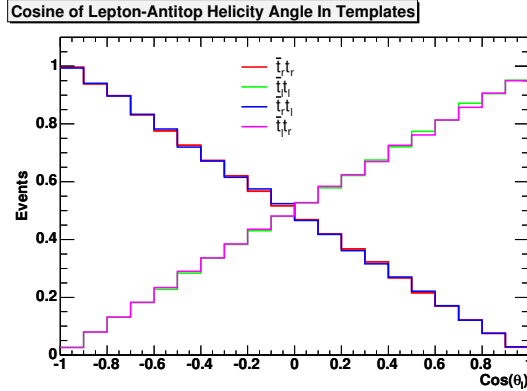


Figure 8: Distribution of $\cos(\theta_l)$ variable in antitop quark decays at truth level for our four samples representing the four different top pair helicity states. The samples show the expected slopes of -1 for right-handed antitops and $+1$ for left-handed antitops.

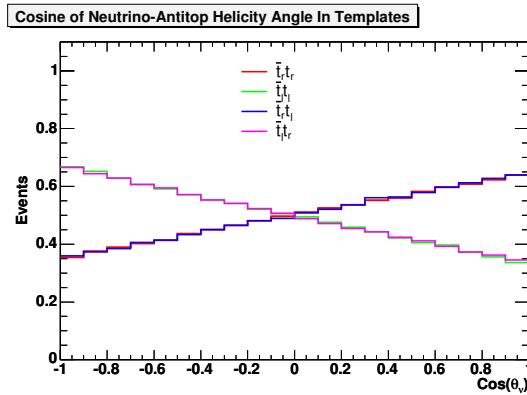


Figure 9: Distribution of $\cos(\theta_\nu)$ variable in antitop quark decays at truth level for our four samples representing the four different top pair helicity states. The samples show the expected slopes of $+0.31$ for right-handed antitops and -0.31 for left-handed antitops.

again show $\cos(\theta_l) \cos(\theta_d)$ at truth level, comparing HERWIG without spin correlations to our same and opposite helicity templates, but in these figures the down quark is chosen using this prescription. This probabilistic choice reduces the difference between our templates and uncorrelated HERWIG, but a significant effect is still present.

3.2 Measurement Method

With the same and opposite helicity templates created, we can use them in performing our fit. Our fitting method is a binned likelihood fit to the data, using three separate templates - the same helicity template, the opposite helicity template, and the background template. The background template was discussed in Section 2, and Figure 15

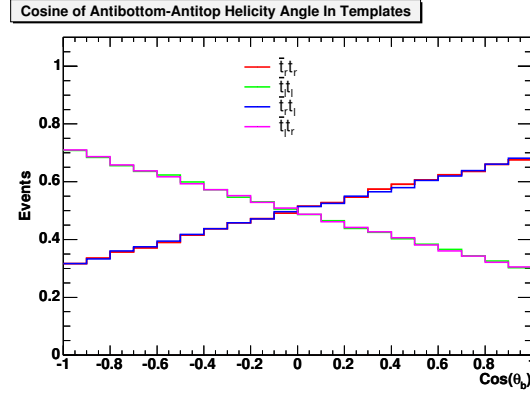


Figure 10: Distribution of $\cos(\theta_b)$ variable in antitop quark decays at truth level for our four samples representing the four different top pair helicity states. The samples show the expected slopes of $+0.41$ for right-handed antitops and -0.41 for left-handed antitops.

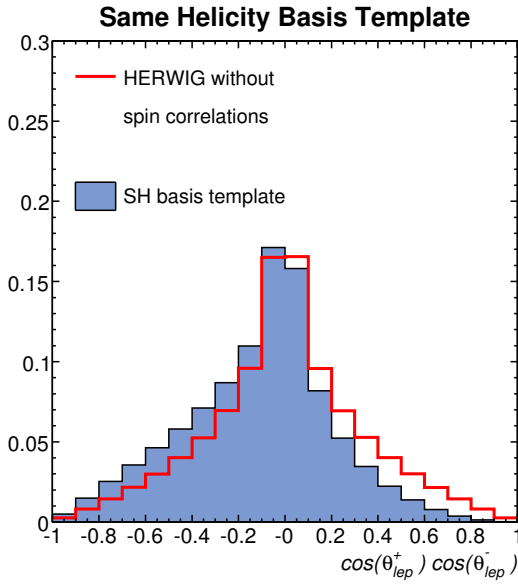


Figure 11: Truth distribution of $\cos(\theta_l) \cos(\theta_d)$ variable in our same helicity sample compared to HERWIG with no spin correlations. Note that the same helicity template tends towards negative values.

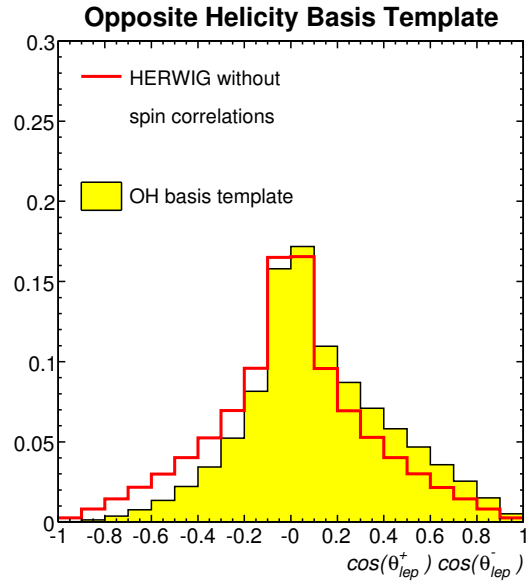


Figure 12: Truth distribution of $\cos(\theta_l) \cos(\theta_d)$ variable in our opposite helicity sample compared to HERWIG with no spin correlations. Note that the opposite helicity template tends towards positive values.

shows the various components that go into this background template, and their relative sizes, for the $\cos(\theta_l) \cos(\theta_d)$ distribution.

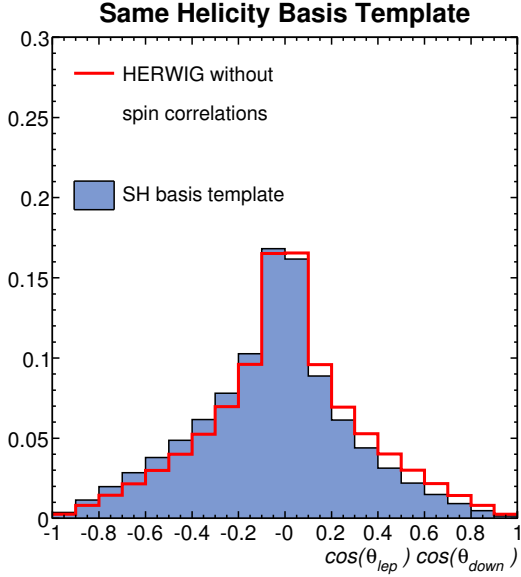


Figure 13: Truth distribution of $\cos(\theta_l)\cos(\theta_d)$ variable in our same helicity sample compared to HERWIG with no spin correlations. The d quark is chosen probabilistically to be the jet closest to the b jet in the W rest frame. Note that the same helicity template still tends towards negative values.

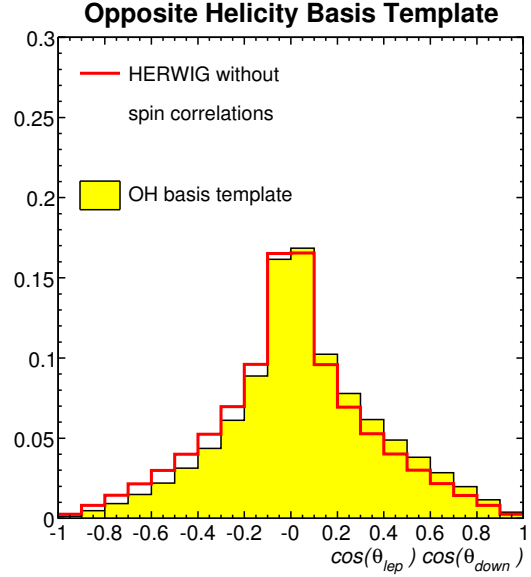


Figure 14: Truth distribution of $\cos(\theta_l)\cos(\theta_d)$ variable in our opposite helicity sample compared to HERWIG with no spin correlations. The d quark is chosen probabilistically to be the jet closest to the b jet in the W rest frame. Note that the opposite helicity template still tends towards positive values.

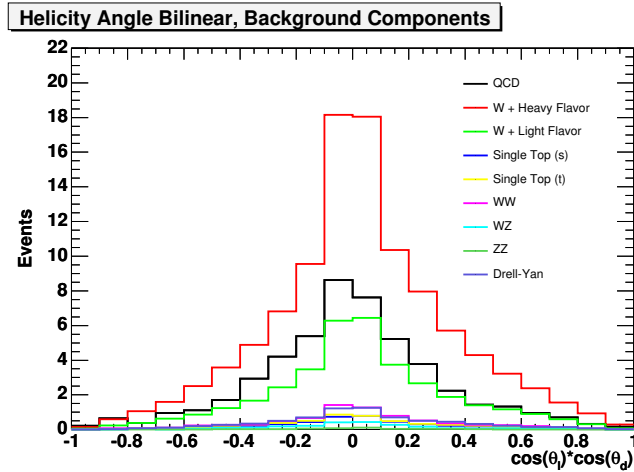


Figure 15: Distribution of the $\cos(\theta_l)\cos(\theta_d)$ variable for the various components of our background template. The largest component of our background model consists of W + heavy flavor jet events.

We consider two separate helicity angle bilinears in our fit, $\cos(\theta_l)\cos(\theta_d)$ and $\cos(\theta_l)\cos(\theta_b)$. Two 1-dimensional likelihood fits could be performed using these two variables, but pseudoexperiments show that there is a significant gain in sensitivity when the two variables are combined into a single 2-dimensional fit, so this is the chosen method for our measurement. When performing the fit, the background normalization is Gaussian-constrained to the predicted value, but the same helicity fraction f_s and opposite helicity fraction f_o are allowed to float freely. We do not require that f_s and f_o be constrained to physical values between 0 and 1, but we do require $f_s + f_o = 1$. Figures 16 and 17 show the mean and pull respectively for pseudoexperiments performed on a sample with an input opposite helicity fraction of 0.70, showing an expected statistical uncertainty of approximately 0.23.

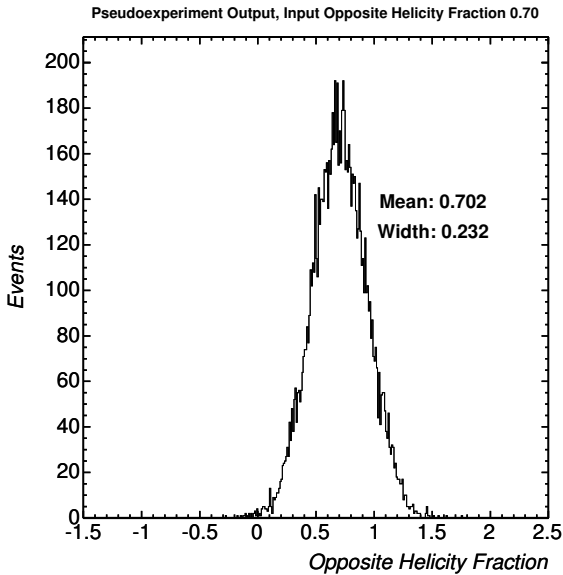


Figure 16: Output from 10000 pseudoexperiments in which our fit was performed using pseudodata based on an input sample with opposite helicity fraction 0.70. This output indicates an expected statistical uncertainty of 0.23.

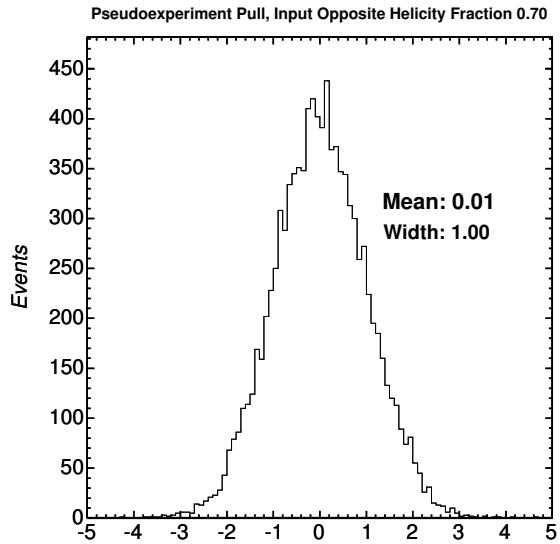


Figure 17: Pseudoexperiment pull from 10000 pseudoexperiments in which our fit was performed using pseudodata based on an input sample with opposite helicity fraction 0.70, indicating that our fit does not introduce any bias.

4 Systematic Uncertainties

There are a number of systematic effects that contribute to our uncertainty which need to be taken into account. These include uncertainties in the background size and shape, uncertainties in the exact detector response, and uncertainties in the underlying structure of the colliding particles. Each of these uncertainties is handled its own unique way, but all follow the same general procedure. We start with a template consisting

of a nominal background and signal model, and then replace either the background or signal model with a model where the appropriate systematic effect has been varied. Our fit is then performed using this new template, and the result compared to the nominal result in order to determine the systematic uncertainty. In all cases, except for the “Bias Around Null” uncertainty, the signal models used had a true opposite helicity fraction of 0.70. The ”Bias Around Null” uncertainty results from a small deviation from the expected fit result of 0.50 for f_o when using a signal sample composed of top pair events where spin correlation effects are not included. It is believed that this deviation is a statistical fluctuation, but we conservatively include it as a systematic uncertainty. The resulting uncertainties from these studies are contained in Table 1.

Systematic	Uncertainty
Bias Around Null	0.0600
JES	0.0423
ISR/FSR	0.0295
Background Shape	0.0225
Color Reconnection	0.0087
PDF	0.0071
Parton Shower	0.0056
Background Size	0.0015
Total Uncertainty	0.0832

Table 1: Summary of Systematic Uncertainties

5 Results

With our fitting procedure established and all systematics uncertainties calculated, the final result of our 2-dimensional fit of $\cos(\theta_l)\cos(\theta_d)$ vs. $\cos(\theta_l)\cos(\theta_b)$ in data corresponding to an integrated luminosity of 4.3fb^{-1} returns an oppsite helicity fraction of

$$f_o = 0.80 \pm 0.25_{\text{stat}} \pm 0.08_{\text{syst}} \quad .$$

Converting this to the spin correlation coefficient using $\kappa = 2 * f_o - 1$ yields

$$\kappa = 0.60 \pm 0.50_{\text{stat}} \pm 0.16_{\text{syst}} \quad .$$

Figures 18 and 19 show the 1-dimensional distributions for $\cos(\theta_l)\cos(\theta_d)$ and $\cos(\theta_l)\cos(\theta_b)$ respectively, where our data is compared to the sum of the background model, same helicity model, and opposite helicity model, with the normalizations determined by the result of our fit for f_o .

Finally, Figures 20 through 22 show the distributions $\cos(\theta_l)$, $\cos(\theta_d)$, and $\cos(\theta_b)$ for the three individual decay products, again comparing the data to the sum of the

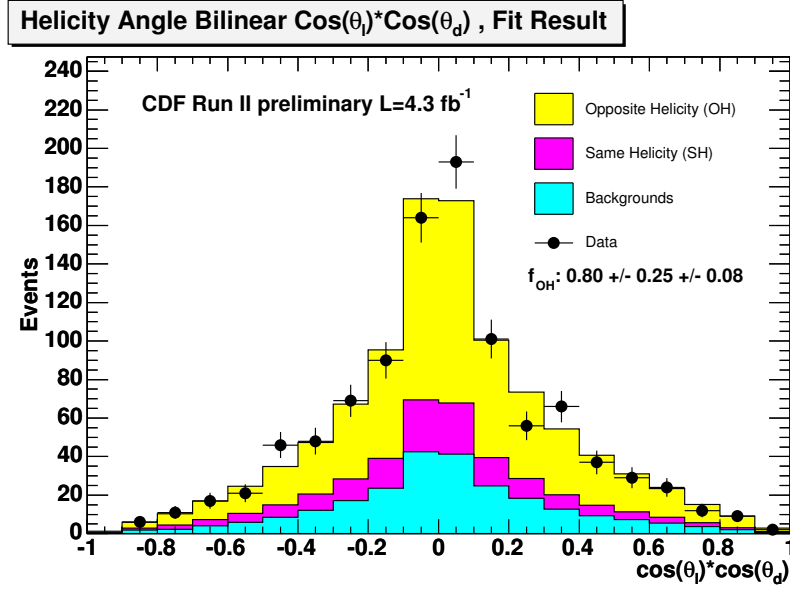


Figure 18: Distribution of the $\cos(\theta_l) \cos(\theta_d)$ variable in data compared to the sum of our background model (light blue), the same helicity template (pink), and the opposite helicity template (yellow), where the opposite helicity fraction in the model is given by $f_o = 0.80$.

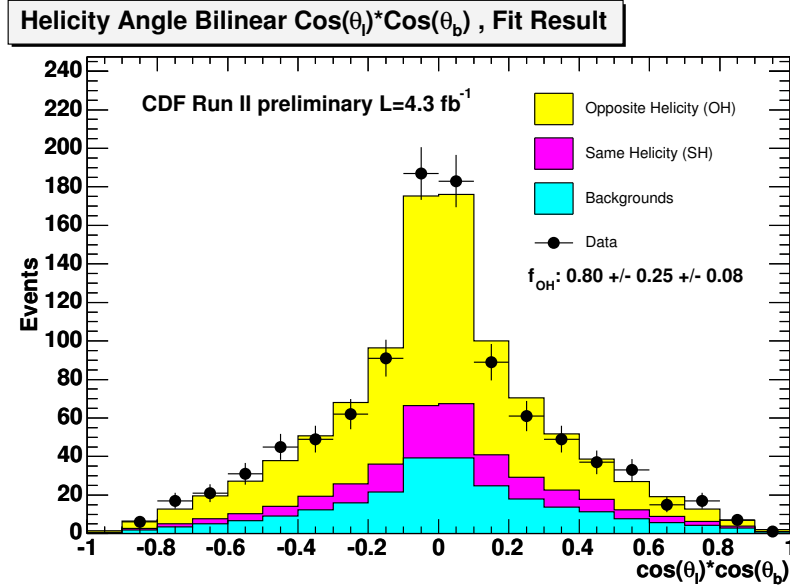


Figure 19: Distribution of the $\cos(\theta_l) \cos(\theta_b)$ variable in data compared to the sum of our background model (light blue), the same helicity template (pink), and the opposite helicity template (yellow), where the opposite helicity fraction in the model is given by $f_o = 0.80$.

background model, same helicity model, and opposite helicity model, with the normalizations determined by the result of our fit for f_o .

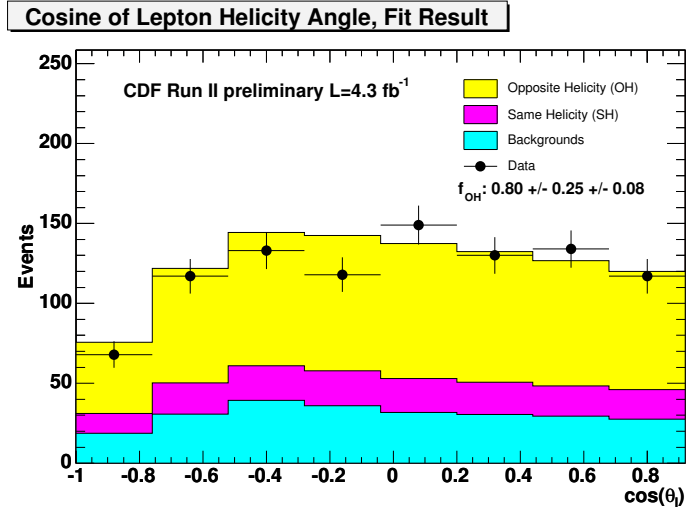


Figure 20: Distribution of the $\cos(\theta_l)$ variable in data compared to the sum of our background model (light blue), the same helicity template (pink), and the opposite helicity template (yellow), where the opposite helicity fraction in the model is given by $f_o = 0.80$.

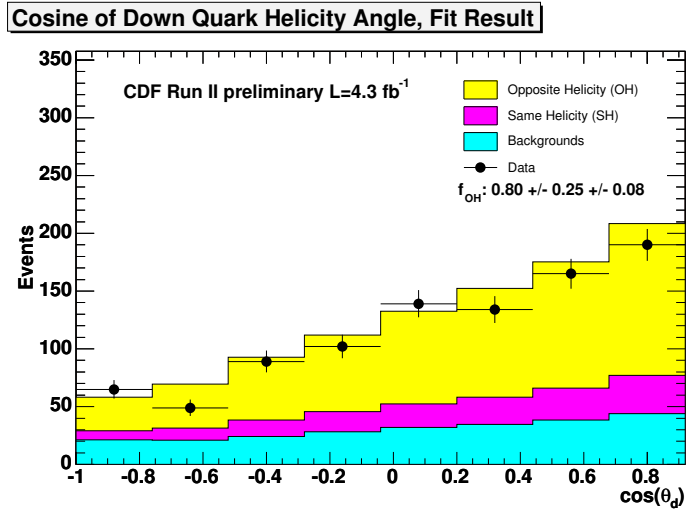


Figure 21: Distribution of the $\cos(\theta_d)$ variable in data compared to the sum of our background model (light blue), the same helicity template (pink), and the opposite helicity template (yellow), where the opposite helicity fraction in the model is given by $f_o = 0.80$.

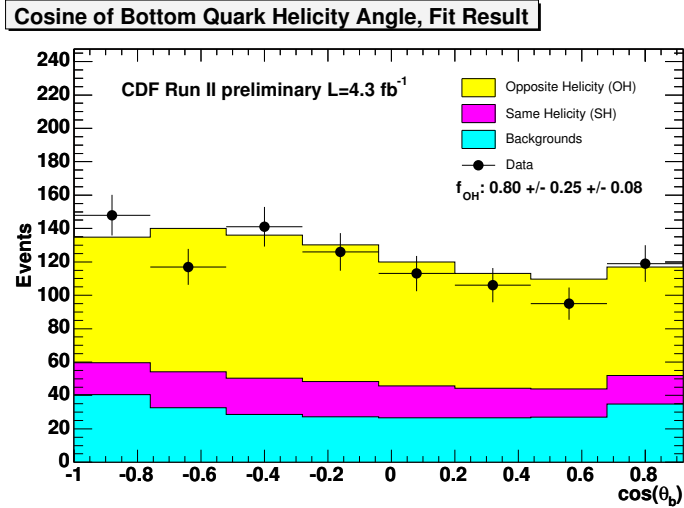


Figure 22: Distribution of the $\cos(\theta_b)$ variable in data compared to the sum of our background model (light blue), the same helicity template (pink), and the opposite helicity template (yellow), where the opposite helicity fraction in the model is given by $f_o = 0.80$.

Acknowledgments

We thank the Fermilab staff and the technical staffs of the participating institutions for their vital contributions. This work was supported by the U.S. Department of Energy and National Science Foundation; the Italian Istituto Nazionale DP Fiske Nucleare; the Ministry of Education, Culture, Sports, Science and Technology of Japan; the Natural Sciences and Engineering Research Council of Canada; the National Science Council of the Republic of China; the Swiss National Science Foundation; the A.P. Sloan Foundation; the Bundesministerium f ur Bildung und Forschung, Germany; the Korean Science and Engineering Foundation and the Korean Research Foundation; the Particle Physics and Astronomy Research Council and the Royal Society, UK; the Institut National de Physique Nucleaire et Physique des Particules/CNRS; the Russian Foundation for Basic Research; the Comisi on Interministerial de Ciencia y Tecnologia, Spain; the European Communitys Human Potential Programme; the Slovak R&D Agency; and the Academy of Finland.

References

- [1] G.L.Kane, G.A.Ladinsky, C.P.Yuan, Phys. Rev. D 45, 124 (1992). 2
- [2] M. Arai, N. Okada, K. Smolek, V. Simak, arXiv:hep-ph/0701155, (2007). 2
- [3] S. Willenbrock, Phys. Lett. B374, 169 (1996). 2
- [4] G. Mahlon and S. parke, Phys. Rev. D 53, 4886 (1996). 2, 4, 6
- [5] The CDF Collaboration, http://www-cdf.fnal.gov/cdfnotes/cdf9824_spincorr2.8fb-1.pdf, June 2009. 2
- [6] The CDF Collaboration, http://www-cdf.fnal.gov/cdfnotes/cdf9724_tbarAfbMeasurement.pdf, March 2009. 3